Available online at www.sciencedirect.com
ScienceDirect
Journal of Sound and Vibration 320 (2009) 942–954
JOURNAL OF SOUND AND VIBRATION
www.elsevier.com/locate/jsvi

Modeling of wave propagation in plate structures using three-dimensional spectral element method for damage detection

Haikuo Peng*, Guang Meng, Fucai Li

State Key Laboratory of Mechanical System and Vibration, Shanghai Jiao Tong University, Shanghai 200240, China

Received 9 July 2008; received in revised form 3 September 2008; accepted 6 September 2008
Handling Editor: L.G. Tham
Available online 11 October 2008

Abstract

This paper presents the application of three-dimensional (3-D) spectral element method (SEM) to wave propagation problems in plate structures for the purpose of damage detection. The excellent characteristic of the SEM is that the mass matrix is diagonal because of the choice of Lagrange interpolation function supported on the Gauss–Lobatto–Legendre (GLL) points in conjunction with the GLL integration rule. Therefore, numerical calculation can be significantly efficient in comparison with the classical finite element method (FEM). By taking advantage of this characteristic, a 3-D spectral finite elements (SFEs)-based model is developed to simulate the wave propagation in plate structures. Lamb waves, propagating in aluminum plates with and without a crack are investigated. Responses from 3-D SFEs- and 2-D SFEs-based models are compared. Different Lamb wave modes are generated using different excitation approaches and, subsequently, characteristics of those modes are analyzed. The results demonstrate that the proposed model can offer efficient and realistic simulation for Lamb wave propagation in plate structures, so as to detect damages in those structures.

1. Introduction

In practical applications of aerospace, civil and mechanical engineering infrastructures, abrupt impact or growth of fatigue defects during the service life can result in catastrophic failure. Hence, various structural health-monitoring techniques have been developed in the literature with the purpose of determining the health status of a system [1]. Recently, elastic wave-based structural monitoring technology has attracted significant attention in the research community. Lamb waves, with the advantages of long-range propagation and sensitivity to a variety of damage types, can serve as an effective mechanism to interrogate plate structures for damage detection [2–7].

Characteristics of the elastic wave propagation are usually required to develop monitoring strategies or interpret damage detection results. A number of numerical methods have been applied to analyze propagation of elastic waves, such as the finite difference method (FDM) [8,9], the finite element method (FEM) [10,11], the

*Corresponding author. Tel.: +86 21 34206664x322; fax: +86 21 34206006.
E-mail address: penghaikuo@gmail.com (H. Peng).

0022-460X/$ - see front matter © 2008 Elsevier Ltd. All rights reserved.
doi:10.1016/j.jsv.2008.09.005

boundary element method (BEM) [12–15], the finite strip elements (FSE) [16,17], the mass-spring lattice model (MSLM) [18–20], and the local interaction simulation approach (LISA) [21–25]. The merits and demerits of each method are discussed by Lee and Staszewski [21,22].

Recently, two different kinds of spectral element method (SEM) have been proposed for analysis of wave propagation, namely, fast Fourier transform (FFT)-based SEM and orthogonal polynomials-based SEM [26,27]. The FFT-based SEM proposed by Doyle [26] is accurate with much less discretization within the model and suited for simple one-dimensional (1-D) or two-dimensional (2-D) problems [28–30]. However, this method becomes inefficient when the problems of the 2-D or 3-D structures with complex geometry are analyzed. On the other hand, the orthogonal polynomials (e.g., Legendre or Cheybysev polynomials)-based SEM, proposed by Patera [27], is much more suitable for analyzing wave propagation in structures with complex geometry. This method is similar to the classical FE method when assembly of element matrices and solution of equations are considered. The difference comes in that orthogonal polynomials are used as approximation functions and, therefore, the mass matrix is diagonal, which is a very significant advantage over FE methods. This method has been successfully applied to many problems such as fluid, seismology and acoustics [31–34]. More recently, the SEM was used to simulate wave propagation in structures for damage detection. For example, wave propagation in 1-D structures, such as rod and beam, were investigated by Sridhar et al. [35] and Kudela et al. [36]. Results of numerical simulation of the transverse elastic wave propagation in a composite plate were presented by Kudela et al. [37]. A 2-D spectral membrane finite element-based model was developed by Zak et al. [38], and was used for the analysis of wave propagation in a cracked isotropic panel.

However, it seems that the application of 3-D SEM to wave propagation problems in damaged structures has not been widely reported in the literature so far. In this paper, a 3-D model on the basis of Legendre polynomials-based spectral finite element is developed and Lamb wave propagation in an aluminum plate is analyzed for damage detection. Lamb wave propagation in the plate with and without a crack is simulated, so as to analyze the influence of the crack. Results from 3-D SFEs- and 2-D SFEs-based models are compared. Finally, characteristics of different Lamb wave modes generated using three excitation approaches are investigated by taking advantage of the proposed model.

2. Formulation of 3-D spectral finite element

The Legendre polynomials-based 3-D spectral finite element discretization proceeds as follows. The domain Ω in three dimensions is firstly meshed to a number of non-overlapping hexahedrons, Ω_e, as in the classical FE method. These elements are subsequently mapped into a reference domain $\Lambda = [-1,1]^3$, a cube in three-dimension, using an invertible local mapping f. On the reference domain Λ, a set of basis functions consisting of Legendre polynomials of degree, N, are introduced, subsequently, a set of nodes are defined. These nodes, denoted by $\xi_i \in [-1,1],\ i \in 1,\ldots,N+1$, are the Gauss–Lobatto–Legendre (GLL) points which are the $(N+1)$ roots of

$$(1-\xi^2)P'_N(\xi) = 0 \tag{1}$$

where $P'_N(\xi)$ is the derivative of the Legendre polynomial of degree N. The definition of element notes result in an irregular distribution of nodes, as shown in Fig. 1, which is different from the classical FE method with uniformly spaced element nodes within elements or on the element boundary.

On the reference domain Λ, the Lagrange interpolation function, u^e_N, supported by the defined nodes, can be expressed as

$$\begin{aligned} u^e_N(\xi,\eta,\gamma) &= \sum_{m=1}^{n_1}\sum_{n=1}^{n_2}\sum_{r=1}^{n_3} u^e_N(\xi_m,\eta_n,\gamma_r)h_m(\xi)h_n(\eta)h_r(\gamma) \\ &= \sum_{m=1}^{n_1}\sum_{n=1}^{n_2}\sum_{r=1}^{n_3} u^e_N(\xi_m,\eta_n,\gamma_r)N_{mnr} \end{aligned} \tag{2}$$

where N_{mnr} is the orthogonal shape functions in 3-D; $h_m(\xi)$ denotes the mth 1-D Lagrange interpolation at the $(N+1)$ GLL points ξ_i introduced above; $h_m(\xi_i)$ equals 1 at $i=m$ and equals 0 at all other points $i \neq m$. From

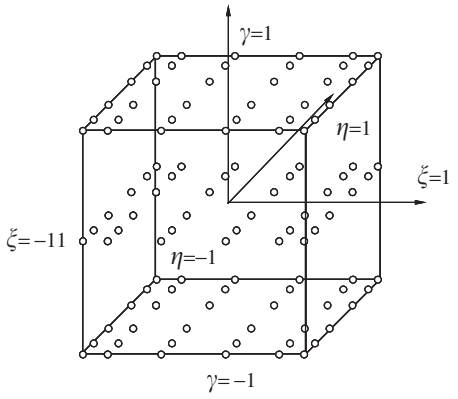

Fig. 1. A 108-node spectral element in the local coordinate.

this definition, we obtain the fundamental property

$$h_m(\xi_i) = \delta_{mi} \tag{3}$$

where δ_{mi} denotes the Kronecker delta. n_i, $i = 1, 2, 3$, is the number of GLL points in each direction in local coordinate.

Similar to the classical FE method, the element matrices, $\mathbf{M}^e$, $\mathbf{K}^e$, and $\mathbf{F}^e$, are calculated numerically as follows:

$$\begin{aligned}\mathbf{M}^e &= \rho \int_{\Omega_e} (\mathbf{N}^e(x,y,z))^{\mathrm{T}} (\mathbf{N}^e(x,y,z))\, \mathrm{d}\Omega_e \\ &= \rho \sum_{i=1}^{n_1} \omega_i \sum_{j=1}^{n_2} \omega_j \sum_{k=1}^{n_3} \omega_k [\mathbf{N}^e(\xi_i,\eta_j,\gamma_k)]^{\mathrm{T}} [\mathbf{N}^e(\xi_i,\eta_j,\gamma_k)] \det[\mathbf{J}_e^{ijk}]\end{aligned} \tag{4}$$

$$\begin{aligned}\mathbf{K}^e &= \int_{\Omega_e} (\mathbf{B}^e(x,y,z))^{\mathrm{T}} \mathbf{D}^e (\mathbf{B}^e(x,y,z))\, \mathrm{d}\Omega_e \\ &= \sum_{i=1}^{n_1} \omega_i \sum_{j=1}^{n_2} \omega_j \sum_{k=1}^{n_3} \omega_k [\mathbf{B}^e(\xi_i,\eta_j,\gamma_k)]^{\mathrm{T}} \mathbf{D}^e [\mathbf{B}^e(\xi_i,\eta_j,\gamma_k)] \det[\mathbf{J}_e^{ijk}]\end{aligned} \tag{5}$$

$$\begin{aligned}\mathbf{F}^e &= \int_{\Omega_e} (\mathbf{N}^e(x,y,z))^{\mathrm{T}} \mathbf{P}\, \mathrm{d}\Omega_e \\ &= \sum_{i=1}^{n_1} \omega_i \sum_{j=1}^{n_2} \omega_j \sum_{k=1}^{n_3} \omega_k [\mathbf{N}^e(\xi_i,\eta_j,\gamma_k)]^{\mathrm{T}} \mathbf{P}(\xi_i,\eta_j,\gamma_k) \det[\mathbf{J}_e^{ijk}]\end{aligned} \tag{6}$$

where ρ is the mass density, $\mathbf{D}^e$ is termed material stiffness matrix [39], and $\mathbf{P}$ is a distributed load. The matrix $\mathbf{B}^e$ is the strain–displacement matrix which can be calculated by

$$\mathbf{B}^e = \mathbf{L}\mathbf{N}^e(\xi_i,\eta_j,\gamma_k) \tag{7}$$

where $\mathbf{L}$ denotes a differential operator matrix:

$$\mathbf{L} = \begin{bmatrix} \partial_x & 0 & 0 & \partial_y & 0 & \partial_z \\ 0 & \partial_y & 0 & \partial_x & \partial_z & 0 \\ 0 & 0 & \partial_z & 0 & \partial_y & \partial_x \end{bmatrix}^{\mathrm{T}}$$

The weights ω_i, independent of the elements, are determined numerically by [40]

$$\omega_i = \frac{2}{n(n-1)[P_{n-1}(\xi_i)]^2}, \quad i \in 1,\ldots,n,\ n = N+1 \tag{8}$$

$\mathbf{J}_e$ is the Jacobian matrix associated with the mapping f from the domain Ω_e to the reference domain Λ:

$$\mathbf{J}_e = \begin{bmatrix} \partial_\xi x & \partial_\xi y & \partial_\xi z \\ \partial_\eta x & \partial_\eta y & \partial_\eta z \\ \partial_\gamma x & \partial_\gamma y & \partial_\gamma z \end{bmatrix}$$

Then the element matrices are assembled to the global coordinate system and a wave propagation modeling problem is transformed to an ordinary differential equation in time. Let $\mathbf{U}$ denote the global vector of unknown displacement in the medium. The ordinary differential equation can be written in a matrix form:

$$\mathbf{M}\ddot{\mathbf{U}} + \mathbf{C}\dot{\mathbf{U}} + \mathbf{K}\mathbf{U} = \mathbf{F} \tag{9}$$

where $\mathbf{M}$ denotes the global mass matrix, $\mathbf{C}$ the global damping matrix, $\mathbf{K}$ the global stiffness matrix, and $\mathbf{F}$ the vector of time-dependent excitation signals.

The second-order ordinary differential equation is solved here using central difference time integration scheme, which is conditionally stable. Zero initial conditions, $\mathbf{U} = 0$ and $\dot{\mathbf{U}} = 0$ at $t = 0$, are assumed to be implemented as initial displacement and velocity field in the central difference time integration scheme [39]:

$$\left(\frac{1}{\Delta t^2}\mathbf{M} + \frac{1}{2\Delta t}\mathbf{C}\right)\mathbf{U}_{t+\Delta t} = \mathbf{F}_t - \left(\mathbf{K} - \frac{2}{\Delta t^2}\mathbf{M}\right)\mathbf{U}_t - \left(\frac{1}{\Delta t^2}\mathbf{M} - \frac{1}{2\Delta t}\mathbf{C}\right)\mathbf{U}_{t-\Delta t} \tag{10}$$

where the symbol t denotes time, Δt denotes the time step of integration. When $\Delta t \leqslant \Delta t_{\mathrm{cr}} = L/c$, the central difference time integration scheme is stable, where L is the minimum distance between two adjacent nodes and c is wave speed in elastic medium.

The excellent characteristics of the SEM used here is that the mass matrix $\mathbf{M}$ is diagonal because of the choice of Lagrange interpolation supported on the GLL points in conjunction with the GLL integration rule, which allows for a significant reduction in the computational effort. It constitutes a major difference compared with classical FEM. The efficiency of SEM was verified using two 3-D models based on SFEs and FEs with the same degrees of freedom and a reduction of about 65% in CPU time used for calculation was observed.

3. Numerical calculations

Lamb waves, propagating in a plate, are investigated using 3-D SFEs illustrated in the previous section. Sketch of the plate with the geometric configuration of 1000 mm × 1000 mm × 2 mm is shown in Fig. 2, which is an aluminum plate (Young's modulus $E = 71\,\mathrm{GPa}$, Poisson ratio $v = 0.33$ and mass density $\rho = 2700\,\mathrm{kg\,m^{-3}}$). In this model, damping is not considered and the boundaries are free. A Hanning-windowed five-cycle sinusoidal toneburst is used as excitation signal. Waveforms of the excitation signal in both the time domain and frequency domain are shown in Fig. 3.

3.1. Lamb wave propagating in aluminum plates

Lamb waves propagating in the aluminum plates with and without a crack are addressed in the present study, using the proposed 3-D SFEs-based model. The plates are meshed to $100 \times 100 \times 1$ SFEs and the number of GLL points in local coordinate is $6 \times 6 \times 3$, as shown in Fig. 1. A through-thickness crack is modeled by reducing element stiffness, as described in [41]. The location and size of the crack are shown in Fig. 2. Length of the crack is 100 mm. It has been assumed that the crack locates 200 mm away from the horizontal center and 50 mm away from the vertical center. Lamb wave is excited using a single shear force with the central frequency of 200 kHz at point A on the upper surface of the plate in the y direction.

The components of displacement response, u_1, in the x direction and, u_2, in the y direction of the plate without and with a crack at the time of 0.050, 0.075, and 0.122 ms are presented in Figs. 4 and 5, respectively. The longitude waves and the shear wave appear under the excitation of the shear force and then are reflected by the boundaries. Significant differences between Figs. 4 and 5 can be observed due to the existence of a crack, and obviously reflections from the direction perpendicular to the crack are dominant.

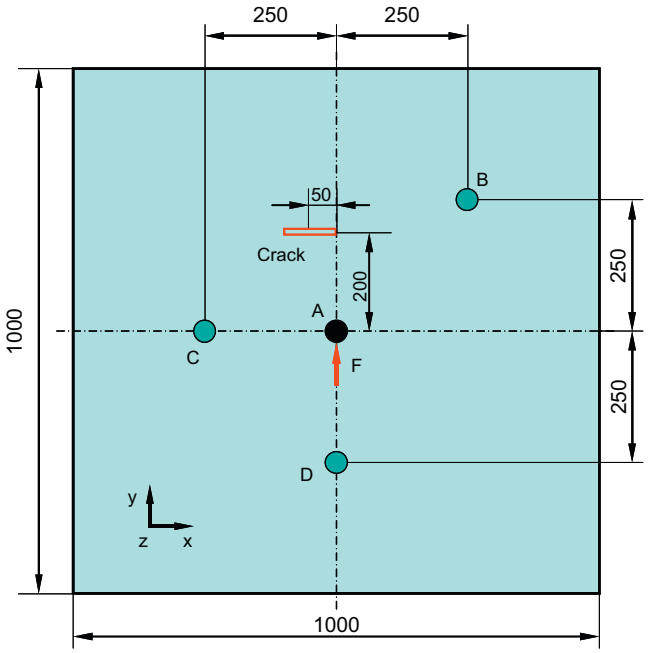

Fig. 2. The geometry of the aluminum plate with a crack (mm).

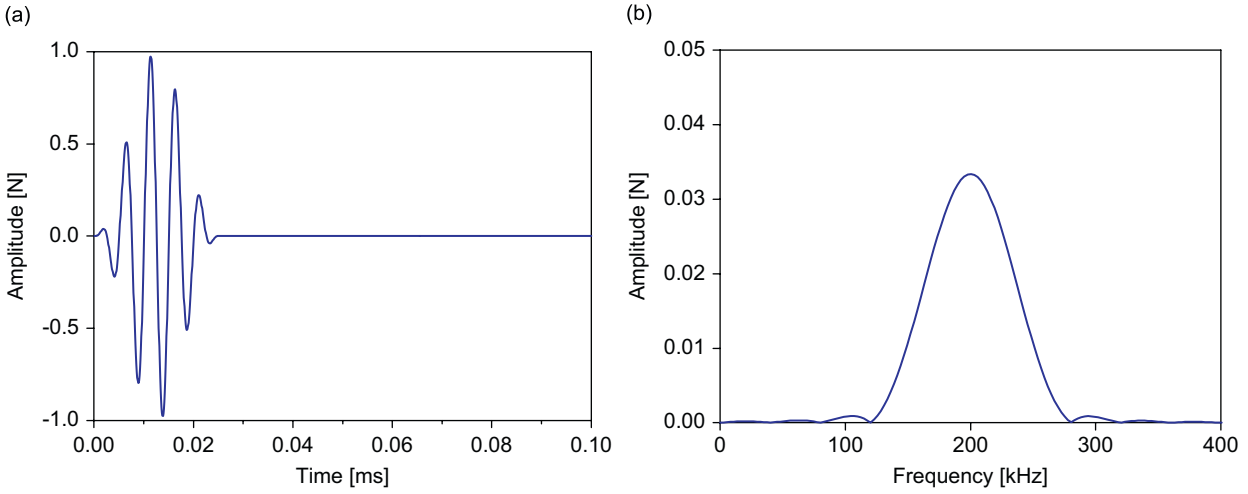

Fig. 3. The waveform (a) in the time domain and (b) in the frequency domain.

The displacement responses at the points B, C, and D on the upper surface, denoted by B', C', and D', respectively, are investigated. To show the wave propagation features of the plate with a crack more clearly, the response of undamaged plate are subtracted from the response of damaged plate. In practical applications, the differences of the responses are usually used in damage detection. The normalized differences of responses are presented in Figs. 6–8. It is obvious that the crack has more influence on displacement response at point C' and D', contrastively, less influence at point B'. This is because the points C' and D' locate under the crack and, therefore, the reflected waves in that direction are dominant. On the contrary, point B' locates right at the crack and a reflected wave with smaller amplitude is captured in that direction.

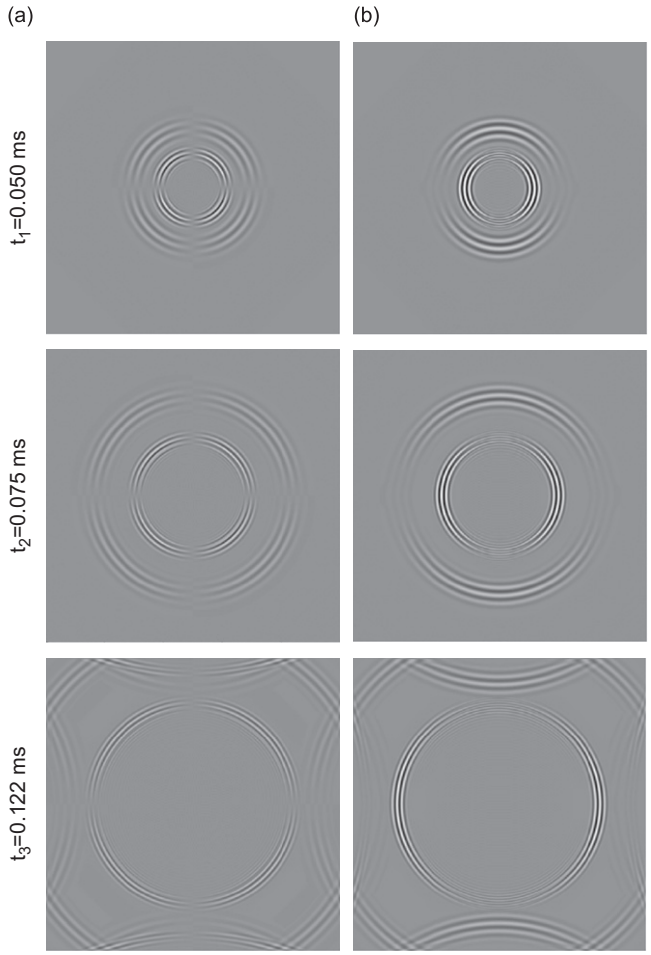

Fig. 4. Displacement responses of the plate without crack: (a) u_1, in the x direction and (b) u_2, in the y direction.

Generally speaking, waves contributed by the damage carry the information of the damage location and size. The information about the damage location relates to the location of the source point A and the measure points (i.e., B', C', and D'), time delay and propagating velocities of those waves. On the other hand, size of the damage is determined by the changes of amplitude of response signals. In engineering applications, a sensor array is usually introduced in the damage detection scheme.

3.2. Comparison with 2-D SFEs

As a comparison, a plate without crack is further modeled using 2-D membrane SFEs proposed in [38], in which 100×100 elements are introduced. The number of GLL points is 6×6. A single shear force parallel to the y direction is applied to the upper surface of point A.

The displacement responses at point B from 3-D and 2-D models are compared. In the 3-D model, two responses are measured on the upper and the lower surfaces of each point, denoted by B' and B'', respectively. A little difference between the responses from 3-D and 2-D models can be observed from Fig. 9(a and b). This is because when the plate is modeled using 3-D SFEs, the thickness of the plate is considered. Meantime, displacement responses of B' and B'' in 3-D model are not always equal. Moreover, displacement component u_3, in the z direction, can be obtained from 3-D model and the symmetric and asymmetric Lamb modes can be observed in that direction, as shown in Fig. 9(c). However, only two in-plane displacements are calculated

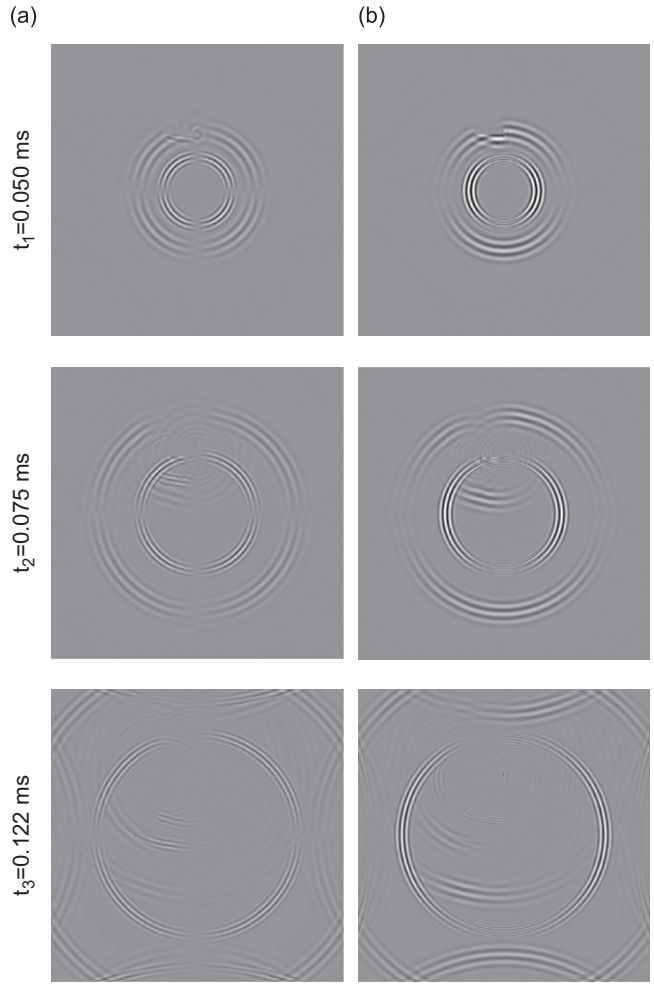

Fig. 5. Displacement responses of the plate with a crack: (a) u_1, in the x direction and (b) u_2, in the y direction.

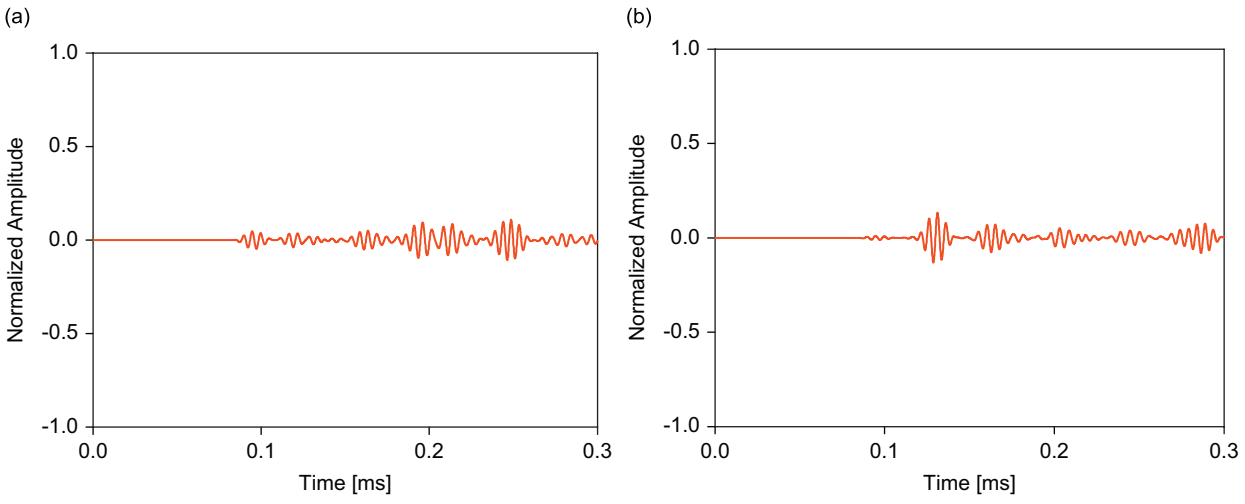

Fig. 6. Normalized differences of displacement responses at point B': (a) u_1, in the x direction and (b) u_2, in the y direction.

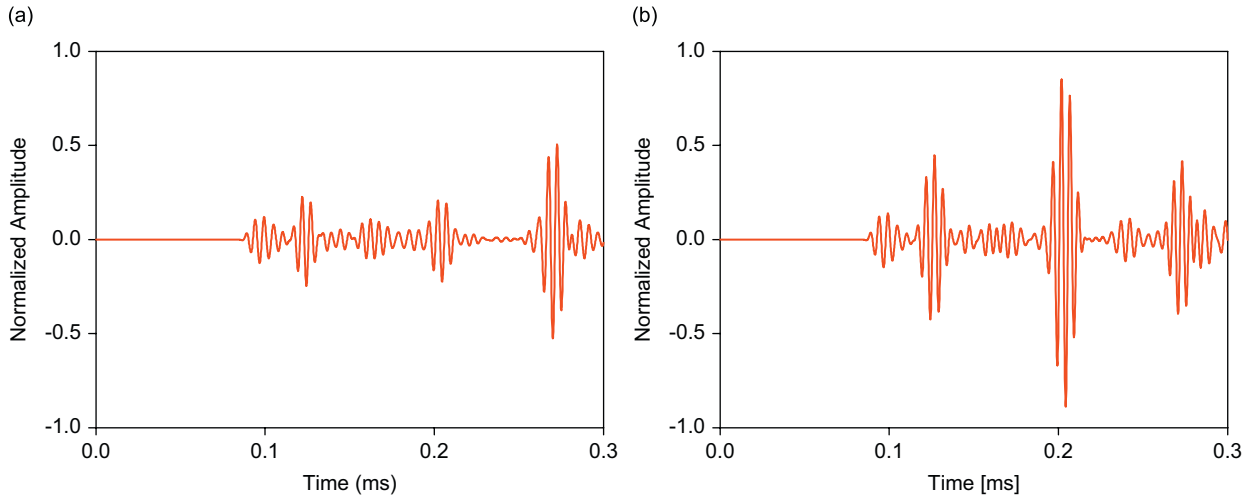

Fig. 7. Normalized differences of displacement responses at point C': (a) u_1, in the x direction and (b) u_2, in the y direction.

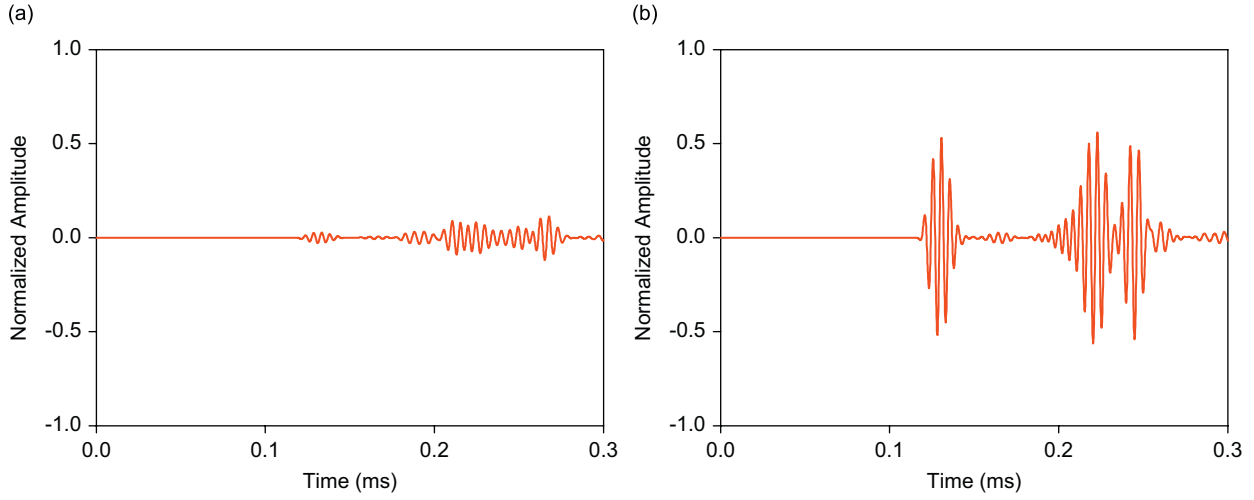

Fig. 8. Normalized differences of displacement responses at point D': (a) u_1, in the x direction and (b) u_2, in the y direction.

within the plate in 2-D model. Therefore, a 3-D SFEs-based model can offer better results than a 2-D SFEs-based model. Additionally, 3-D SFEs have a potential to model structures with more complex geometry.

3.3. Generation of different Lamb wave modes

The 3-D SFEs provide an efficient tool in analyzing the propagation characteristics of different Lamb wave modes. In most cases, multiple Lamb modes exist simultaneously and, moreover, dispersive properties of those Lamb modes are not identical even for the same mode in different frequency ranges. It is necessary to carry out the damage detection strategies based on a certain wave propagation mode. Practically, the fundamental symmetric Lamb wave mode, S0, and the fundamental asymmetric Lamb wave mode, A0, are usually used for damage detection in plate structures. In this section, the Lamb modes are generated with three excitation approaches, as shown in Fig. 10, in the aluminum plate modeled by 3-D SFEs. The results are shown in Figs. 11 and 12.

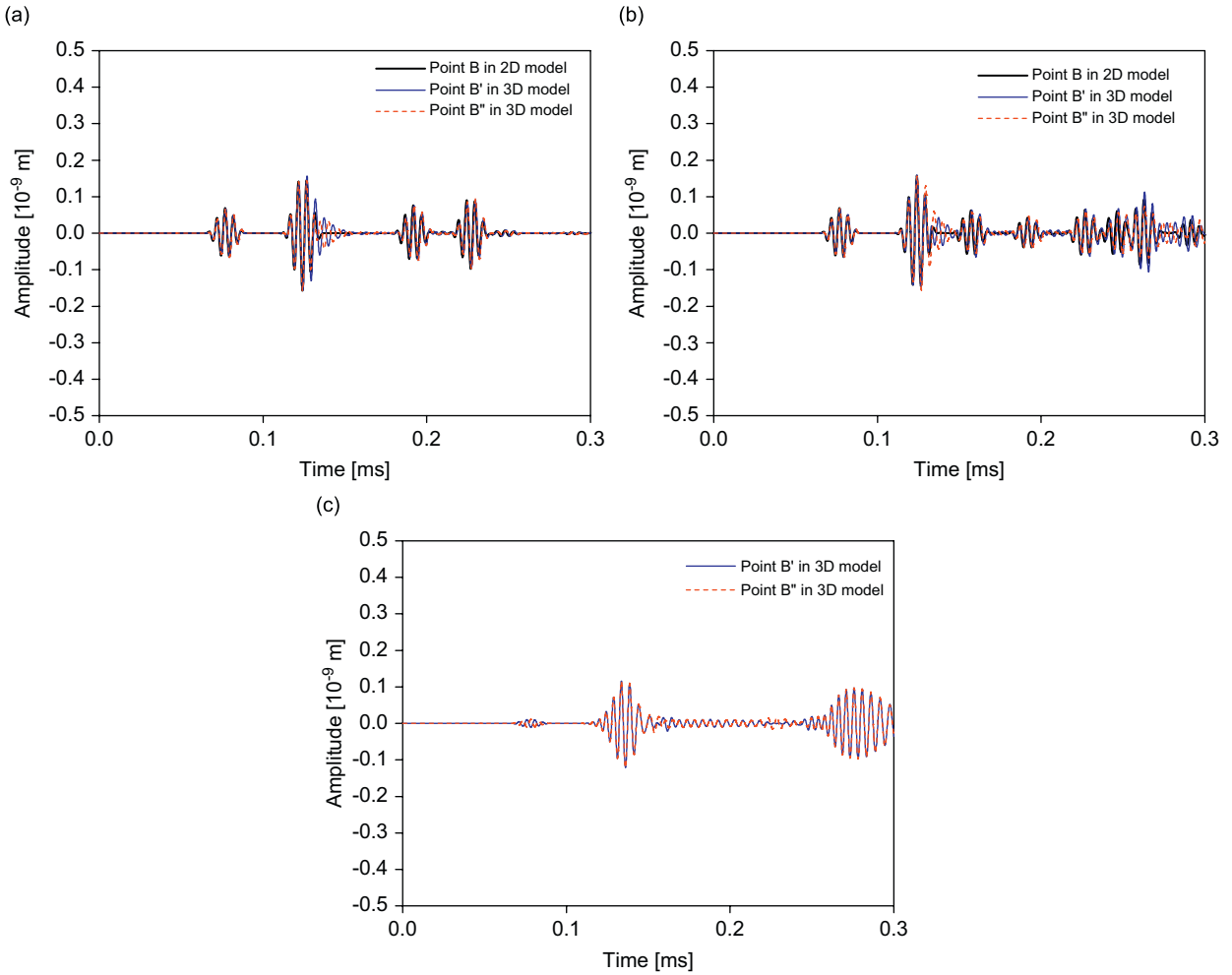

Fig. 9. Comparison of displacement responses from 3-D and 2-D SFE models at point B: (a) u_1, in the x direction; (b) u_2, in the y direction; and (c) u_3, in the z direction.

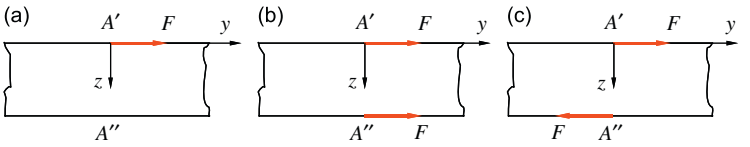

Fig. 10. Excitation approaches of: (a) case 1, a single shear force, (b) case 2, dual forces with the same direction, and (c) case 3, dual forces with the opposite direction.

In case 1, a single shear force, parallel to the y direction, is applied on the upper surface at point A of the plate, as used in the previous section. The responses at the points B' on the upper surface are displayed in Figs. 11 and 12, where the symmetric Lamb mode, S0, the shear mode, SH0, and the symmetric mode, A0, simultaneously exist.

In case 2, dual forces with the same direction are applied on both the upper surface and lower surface of the plate at point A. The symmetric Lamb mode, S0, and the shear mode, SH0, can be seen with enhanced amplitudes, indicating that stronger wave energy is centralized on the S0 mode and the SH0 mode. Meanwhile, the asymmetric mode, A0, cannot be observed.

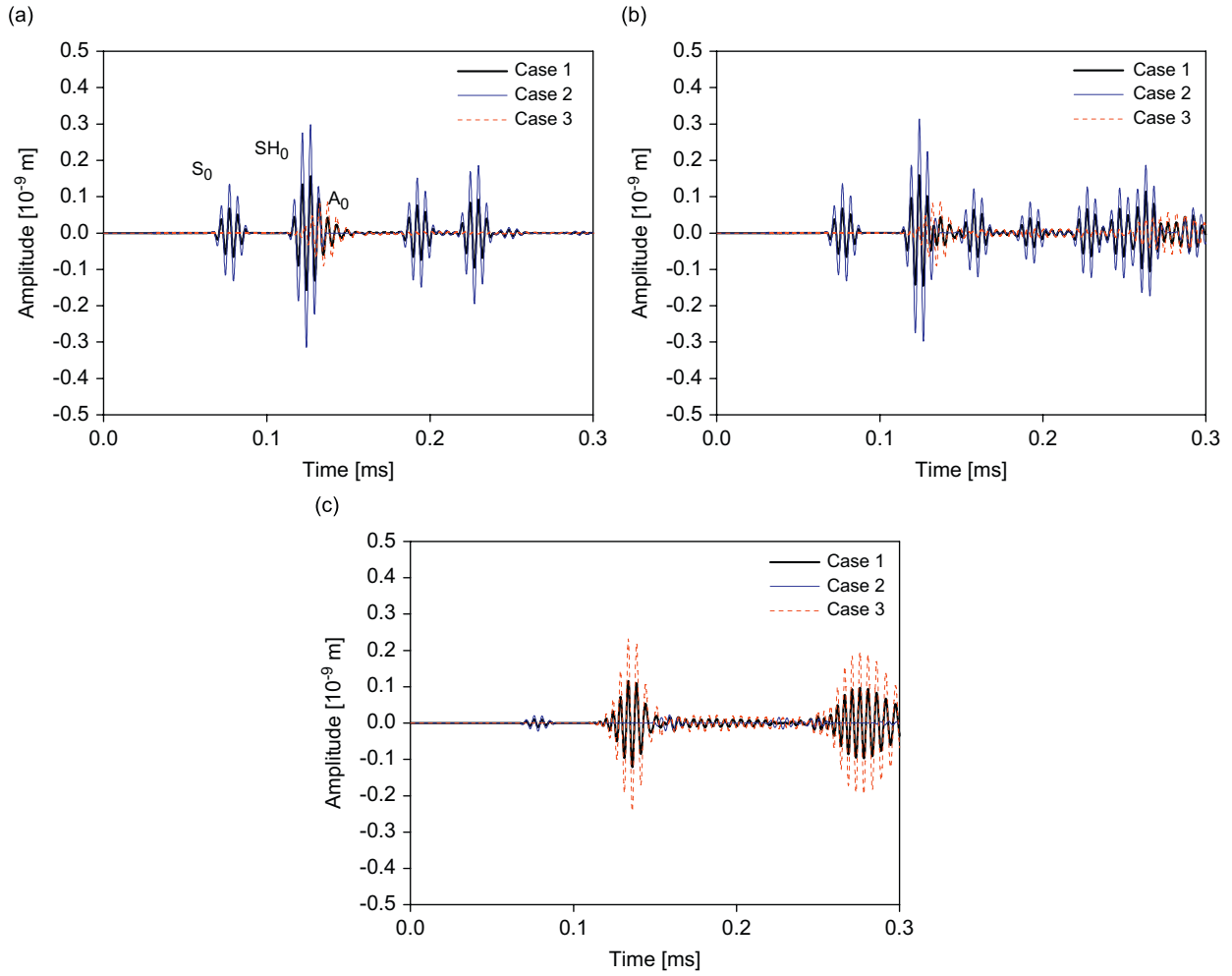

Fig. 11. Displacement responses at point B' under different excitation approaches (central frequency of excitation is 200 kHz): (a) u_1, in the x direction, (b) u_2, in the y direction, and (c) u_3, in the z direction.

In case 3, when the dual forces with the opposite direction, are applied, the asymmetric mode, A0, is observed to be dominant, while the symmetric mode and the shear wave mode are suppressed. We can see that the A0 mode has a deformed shape with about 10-cycle signal compared with the 5-cycle excitation signal, while the S0 and the SH0 mode keep their original shapes.

Group velocities of different Lamb wave modes are usually not identical. It is evident from Figs. 11 and 12 that the group velocity of the SH0 mode is smaller than that of the S0 mode, but a little larger than that of the A0 mode. Even, group velocities of single Lamb wave mode excited by signals with different central frequencies are different. According to Figs. 11 and 12, the group velocity of the A0 mode is obviously different under the applied excitation with central frequencies 100 and 200 kHz, but there is no obvious difference in group velocities of S0 and SH0 modes. In fact, the relation between group velocity and central frequency of applied excitation can be illustrated using dispersion curves, as shown in Fig. 13. Those dispersion curves also demonstrate the effectiveness of the proposed model because of the good agreement between the analytical and simulated results in the frequency band of 0 Hz–300 kHz.

The symmetric or asymmetric Lamb wave modes are easily excited using the model based on the 3-D SFEs and, therefore, the model can be significantly helpful in understanding the wave propagation phenomena, as well as developing damage detection strategies and interpreting the features.

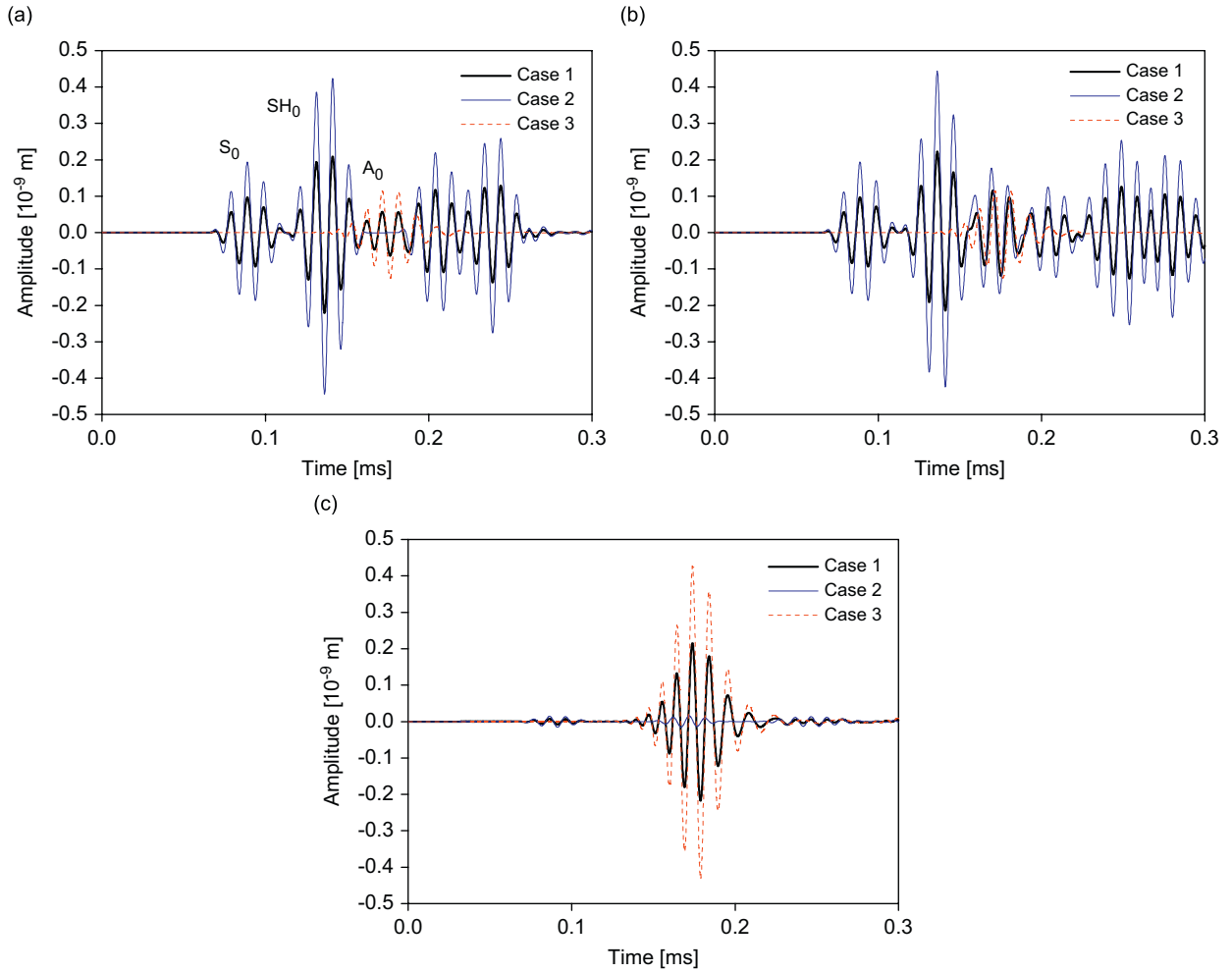

Fig. 12. Displacement responses at point B' under different excitation approaches (central frequency of excitation is 100 kHz): (a) u_1, in the x direction, (b) u_2, in the y direction, and (c) u_3, in the z direction.

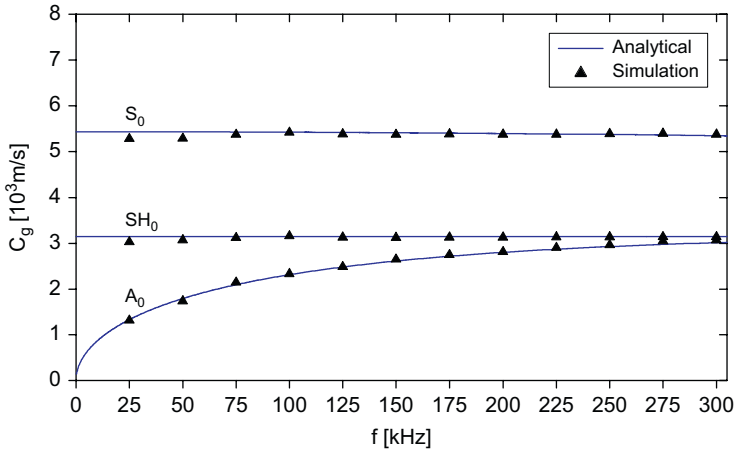

Fig. 13. Dispersion curves in the frequency band 0 Hz–300 kHz using analytical and simulated methods.

4. Conclusion

Interpretation of captured responses plays a vital role in Lamb wave-based damage detection. Lamb wave propagation in aluminum plates with and without a crack modeled by 3-D SFEs is simulated in the present study. The results obtained from 3-D SFE- and 2-D SFE-based model are compared. Characteristics of different Lamb modes are therefore analyzed.

The present work shows that the 3-D SFEs provide an efficient tool to analyze wave propagation in structures for damage detection. The advantages of the proposed model can be summarized as follows: (1) The structures and the damages with complex geometry can be conveniently modeled using 3-D SFEs; (2) calculation can be significantly efficient in comparison with classical FEM because of the diagonal form of element mass matrix; (3) compared with 2-D SFEs, the 3-D SFEs can be more precisely and realistically model the physical structures; therefore better results can be offered; (4) the generation of different Lamb wave modes can be easily carried out by the 3-D SFEs-based model, therefore it can be significantly helpful in developing damage detection strategies since a certain Lamb mode is usually used in practical implementation. In summary, the proposed model can offer efficient and realistic simulation for Lamb wave propagation in plate structures, so as to detect damage in those structures.

The 3-D SFEs will be extended to simulate Lamb wave propagation in multilayer composite plates or Rayleigh wave in 3-D structures with more complex geometry for damage detection in the future work.

Acknowledgments

The authors are grateful for the support received from the Natural Science Foundation of China (NSFC Nos. 10702041 and 10528206) and Key International S&T Cooperation Project of China Ministry of Science and Technology (No. 2005DFA00110).

References

[1] D.J. Inman, C.R. Farrar, J.V. Lopes, J.V. Steffen, *Damage Prognosis for Aerospace, Civil and Mechanical Systems*, Wiley, New York, 2004.
[2] D.C. Worlton, Experimental confirmation of Lamb waves at megacycle frequencies, *Journal of Applied Physics* 32 (1961) 967–971.
[3] D.N. Alleyne, P. Cawley, The interaction of Lamb waves with defects, *IEEE Transactions on Ultrasonics, Ferroelectrics and Frequency Control* 39 (3) (1992) 381–397.
[4] E. Moulin, J. Assaad, C. Delebarre, D. Osmont, Modeling of Lamb waves generated by integrated transducers in composite plates using a coupled finite element-normal modes expansion method, *The Journal of the Acoustical Society of America* 107 (1) (2000) 87–94.
[5] S.S. Kessler, S.M. Spearing, C. Soutis, Damage detection in composite materials using Lamb wave methods, *Smart Materials and Structures* 11 (2) (2002) 269–278.
[6] V. Giurgiutiu, Tuned Lamb wave excitation and detection with piezoelectric wafer active sensors for structural health monitoring, *Journal of Intelligent Material Systems and Structures* 16 (2005) 291–305.
[7] Z. Su, L. Ye, Y. Lu, Guided Lamb waves for identification of damage in composite structures: a review, *Journal of Sound and Vibration* 295 (2006) 753–780.
[8] J.C. Strikwerda, *Finite Difference Schemes and Partial Differential Equations*, Wadsworth Publ. Co., Belmont, CA, 1989.
[9] Z.Z. Sun, X. Wu, A fully discrete difference scheme for a diffusion-wave system, *Applied Numerical Mathematics* 56 (2) (2006) 193–209.
[10] O.C. Zienkiewicz, *The Finite Element Method*, fourth ed., McGraw-Hill, London, 1989.
[11] N. Guo, P. Cawley, The interaction of Lamb waves with delaminations in composite laminates, *The Journal of the Acoustical Society of America* 94 (4) (1993) 2240–2246.
[12] Y. Cho, J.L. Rose, A boundary element solution for a mode conversion study on the edge reflection of Lamb waves, *The Journal of the Acoustical Society of America* 99 (4) (1996) 2097–2109.
[13] L. Vernhet, Boundary element solution of a scattering problem involving a generalized impedance boundary condition, *Mathematical Methods in the Applied Sciences* 22 (7) (1999) 587–603.
[14] L. Wang, J. Shen, Scattering of elastic waves by a crack in a isotropic plate, *Ultrasonic* 35 (6) (1997) 451–457.
[15] X. Zhao, J. Rose, Boundary element modeling for defect characterization potential in a wave guide, *International Journal of Solids and Structures* 40 (11) (2003) 2645–2658.
[16] B. Alessio, B. Fabio, Finite strip modeling for optimal design of prestressed folded plate structures, *Engineering Structures* 26 (8) (2004) 1043–1054.

[17] D.J. Dawe, Use of the finite strip method in predicting the behaviour of composite laminated structures, *Composite Structures* 57 (1–4) (2002) 11–36.
[18] Y. Sohn, S. Krishnaswamy, Mass spring lattice modeling of the scanning laser source technique, *Ultrasonics* 39 (8) (2002) 543–551.
[19] H. Yim, Y. Sohn, Numerical simulation and visualization of elastic waves using mass-spring lattice model, *IEEE Transactions on Ultrasonics, Ferroelectrics and Frequency Control* 47 (3) (2000) 549–558.
[20] P.P. Delsanto, M. Scalerandi, A spring model for the simulation of the propagation of the ultrasonic pulses through imperfect contact interfaces, *The Journal of the Acoustical Society of America* 104 (5) (1998) 2584–2591.
[21] B.C. Lee, W.J. Staszewski, Lamb wave propagation modelling for damage detection: I. Two-dimensional analysis, *Smart Materials and Structures* 16 (2) (2007) 249–259.
[22] B.C. Lee, W.J. Staszewski, Lamb wave propagation modelling for damage detection: II. Damage monitoring strategy, *Smart Materials and Structures* 16 (2) (2007) 260–274.
[23] P.P. Delsanto, T. Whitcombe, H.H. Chaskelis, R.B. Mignogna, Connection machine simulation of ultrasonic wave propagation in materials. I: the one-dimensional case, *Wave Motion* 16 (1992) 65–80.
[24] P.P. Delsanto, R.S. Schechter, H.H. Chaskelis, R.B. Mignogna, R. Kline, Connection machine simulation of ultrasonic wave propagation in materials. II: the two-dimensional case, *Wave Motion* 20 (1994) 295–314.
[25] P.P. Delsanto, R.S. Schechter, R.B. Mignogna, Connection machine simulation of ultrasonic wave propagation in materials. III: the three dimensional case, *Wave Motion* 26 (1997) 329–339.
[26] J.F. Doyle, *Wave Propagation in Structures*, Springer, New York, 1989.
[27] A.T. Patera, A spectral element method for fluid dynamics: laminar flow in a channel expansion, *Journal of Computational Physics* 54 (1984) 468–488.
[28] M. Krawczuk, M. Palacz, W. Ostachowicz, The dynamic analysis of cracked Timoshenko beam by the spectral element method, *Journal of Sound and Vibration* 264 (2003) 1139–1153.
[29] D.R. Mahapatra, S. Gopalakrishnan, A spectral finite element model for analysis of axial-flexural-shear coupled wave propagation in laminated composite beams, *Composite Structures* 59 (1) (2003) 67–88.
[30] M. Palacz, M. Krawczuk, Analysis of longitudinal wave propagation in a cracked rod by the spectral element method, *Computers and Structures* 80 (24) (2002) 1809–1816.
[31] G. Seriani, 3-D large scale wave propagation modelling by spectral element method on Cray T3E multiprocessor, *Computer methods in Applied Mechanics and Engineering* 164 (1–2) (1998) 235–247.
[32] D. Komatitsch, C. Barnes, J. Tromp, Simulation of anisotropic wave propagation based upon a spectral element method, *Geophysics* 65 (4) (2000) 1251–1260.
[33] C. Canuto, A. Quarteroni, M.Y. Hussaini, T.A. Zang, *Spectral Methods in Fluid Dynamics*, Springer, Berlin, 1988.
[34] D. Komatitsch, J. Tromp, Introduction to the spectral element method for three-dimensional seismic wave propagation, *Geophysical Journal International* 139 (3) (1999) 806–822.
[35] R. Sridhar, A. Chakraborty, S. Gopalakrishnan, Wave propagation analysis in a anisotropic and inhomogeneous uncracked and cracked structures using pseudospectral finite element method, *International Journal of Solids and Structures* 43 (16) (2006) 4997–5031.
[36] P. Kudela, M. Krawczuk, W. Ostachowicz, Wave propagation modelling in 1D structures using spectral finite elements, *Journal of Sound and Vibration* 300 (2007) 88–100.
[37] P. Kudela, A. Zak, M. Krawczuk, W. Ostachowicz, Modelling of wave propagation in composite plates using the time domain spectral element method, *Journal of Sound and Vibration* 302 (2007) 728–745.
[38] A. Zak, M. Krawczuk, W. Ostachowicz, Propagation of in-plane waves in an isotropic panel with a crack, *Finite Elements in Analysis and Design* 42 (11) (2006) 929–941.
[39] X. Wang, The Finite Element Method, Beijing, 2003.
[40] 〈http://mathworld.wolfram.com〉.
[41] M.I. Friswell, J. Penny, Crack modeling for structural health monitoring, *Structural Health Monitoring* 1 (2) (2002) 139–148.